

Measured Velocity Boundary Layers in Turbulent Convection

Y.-B. Xin and K.-Q. Xia

Department of Physics, The Chinese University of Hong Kong, Shatin, New Territories, Hong Kong

P. Tong

Department of Physics, Oklahoma State University, Stillwater, Oklahoma 74078

(Received 22 August 1995)

Direct measurements of the velocity boundary layer in turbulent convection have been carried out using a novel light scattering technique. The experiment reveals that the velocity profile $v_h(z)$ as a function of the distance z from the lower surface of a convection cell has an invariant form $v_h(z) = v_m f(z/\delta_v)$ over varying Rayleigh numbers (Ra). It is found that the scaling velocity v_m , the viscous boundary layer thickness δ_v , and the shear rate γ all obey power laws of Ra, i.e., $v_m \sim \text{Ra}^{0.5}$, $\delta_v \sim \text{Ra}^{-0.16}$, and $\gamma \sim \text{Ra}^{0.66}$. [S0031-9007(96)00765-X]

PACS numbers: 47.27.Te, 05.40.+j, 42.25.-p

The discovery of the hard turbulence regime [1] in Rayleigh-Bénard convection has attracted much attention in recent years [2]. The hard turbulence state at the Rayleigh number $\text{Ra} > 4 \times 10^7$ is characterized by scaling laws in the heat flux and temperature statistics and also by a coherent large-scale circulation that spans the height of the convection cell. It has been widely recognized that the thermal and viscous boundary layers near the upper and lower surfaces of the cell play an important role in determining the heat flux and temperature statistics [3–5]. Direct measurements of the boundary layer properties, therefore, become essential to the understanding of convective turbulence. In contrast to many thermal boundary layer measurements [3,4,6], however, experimental information about viscous boundary layers in turbulent convection is limited. The lack of the velocity information is partially due to the fact that the conventional methods for measuring velocity, such as hot-wire anemometry and laser Doppler velocimetry (LDV), are not suitable for thermal turbulence. Recently, Tilgner *et al.* have used an imaging technique to measure the velocity profile near the top plate of a cubic cell filled with water [6]. Because of the cumbersome procedure of the method, the velocity measurements were conducted only at a single value of Ra ($\approx 10^9$).

In this Letter we report results of direct measurements of the velocity boundary layer properties for turbulent convection in water with Ra ranging from 10^8 to 10^{10} . A novel light scattering technique of dual-beam cross-correlation spectroscopy [7] is used to measure the velocity profile $v(z)$ as a function of the distance z from the lower surface of the cell. In the experiment two parallel laser beams with a known separation l are shone through the convecting fluid. The two beams are the blue and green lights from an argon-ion laser operated under the multiline mode. The fluid is seeded with neutrally buoyant latex spheres of $0.95 \mu\text{m}$ in diameter. These particles scatter light and follow the motion of the fluid. The velocity of the seed particles is determined

by measuring the time required for the particles to cross the two parallel beams in succession. Experimentally, this transit time is obtained from the cross-correlation function

$$g_c(t) = \frac{\langle I_b(t') I_g(t' + t) \rangle}{\langle I_b(t') \rangle \langle I_g(t') \rangle} = 1 + \beta G_c(t), \quad (1)$$

between the scattered intensities, $I_b(t)$ and $I_g(t)$, from the blue and green beams, respectively. In Eq. (1), $\beta (\leq 1)$ is an instrumental constant. Because there is no phase coherence between I_b and I_g , $g_c(t)$ is sensitive only to the scattering amplitude fluctuations produced by the seed particles moving in and out of the laser beams. For a uniform flow with the velocity v in the direction perpendicular to the laser beams, $G_c(t)$ in Eq. (1) has the form [7] $G_c(t) = \frac{1}{N} e^{-[(vt-\ell)/r_0]^2}$, where r_0 is the radius of the beams and N is the average number of the particles in the scattering volumes. For a turbulent flow $G_c(t)$ becomes [7]

$$G_c(t) = \frac{1}{N} \int dv P(v) e^{-[(vt-\ell)/r_0]^2} \\ = \frac{e^{-(v_0 t - \ell)^2 / [r_0^2 + 2(\sigma t)^2]}}{N \sqrt{1 + 2(\sigma t / r_0)^2}}. \quad (2)$$

In the above, the probability density function (PDF) $P(v)$ of the local velocity v has been assumed to be of a Gaussian form with v_0 being the mean velocity and σ the standard deviation. Because it can distinguish which of the two parallel beams a seed particle traverses first, the dual-beam method is sensitive to the flow direction.

The convection cell used in our experiment was vertical cylinder with its inner diameter and height being 19 and 19.6 cm, respectively. The upper and lower plates were made of copper, and their surfaces were gold plated. The sidewall of the cell was cylindrical ring made of transparent Plexiglas to admit the incident light and transmit the scattered light. The temperature of the upper

plate was regulated by passing cold water through a cooling chamber fitted on the top of the plate. The lower plate was heated uniformly at a constant rate with an embedded film heater. The temperature difference ΔT between the two plates was measured by two thermistors embedded in the plates. The control parameter in the experiment is the Rayleigh number $Ra = \alpha g h^3 \Delta T / \nu \kappa$, with α being the thermal expansion coefficient, g the gravitational acceleration, h the height of the cell, and ν and κ the kinematic viscosity and the thermal diffusivity of the fluid, respectively. Our measurements of the Nusselt number Nu (the normalized heat flux) as a function Ra can be well fitted by the power law $Nu = (0.14 \pm 0.01)Ra^{0.29 \pm 0.004}$, when $10^8 \leq Ra \leq 2 \times 10^{10}$. The measured scaling exponent agrees well with previous measurements [1,3,8].

The optical setup of the experiment has been detailed elsewhere [7], and here we only mention some key points. A lens was used to focus the two laser beams emerging from a prism into the convection cell. The two beams become parallel after passing through the lens, and they were horizontally shone through the center of the cell. A second lens was placed at 90° with respect to the incident direction of the beams, and projected the image of the scattered beams in the cell onto an adjustable slit with a 1:1 magnification. The width of the slit was set at 0.3 mm. The slit was so positioned that only the center portion of the scattered beams was seen by two photomultipliers (PM), which were placed far behind the slit. Aided by a beam splitter and two interference filters, the two PM's were used to record $I_b(t)$ and $I_g(t)$, respectively. The output pulse trains from the two PM's were fed to a digital correlator, which gives $g_c(t)$. Because the acceptance angle of the receiving optics is large enough, small amplitude beam wandering in the convecting fluid will not affect the measurement of $g_c(t)$. The entire convection cell sat on a rotation-translational platform, with which one could rotate the cell about its central vertical axis to change the direction of the large-scale flow relative to the incident laser beams. The cell could also be moved vertically to change the distance z between the beams and the lower surface of the cell. The orientation of the plane defined by the two beams was adjusted to be either parallel or perpendicular to the lower surface, so that the horizontal and vertical components of the velocity could be measured, respectively. The beam separation l was fixed at 0.22 ± 0.01 mm.

Figure 1 shows two cross-correlation functions measured simultaneously at $Ra = 1.8 \times 10^9$, with the correlator being operated under the "dual-cross" mode. The circles represent a "green-cross-blue" (GCB) correlation function $\langle I_g(t')I_b(t'+t) \rangle$, in which the measured $I_g(t)$ was delayed relative to $I_b(t)$. The squares represent a "blue-cross-green" (BCG) correlation function $\langle I_b(t')I_g(t'+t) \rangle$. In this measurement the two beams were oriented such that only the horizontal velocity v_h directly above the center of the lower plate at $z = 3.0$ mm

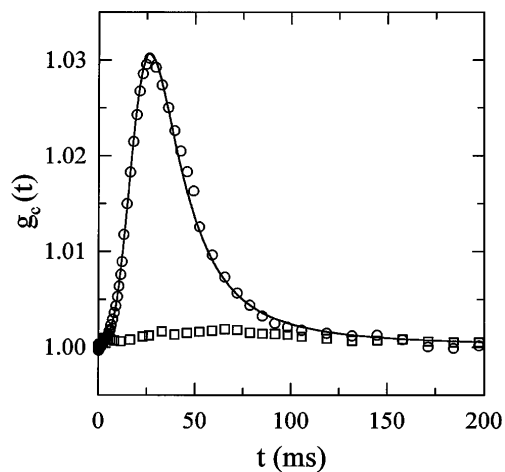


FIG. 1. Measured GCB (circles) and BCG (squares) cross-correlation functions $g_c(t)$ at $Ra = 1.82 \times 10^9$ and $z = 3.0$ mm. The solid curve is a fit by Eq. (2).

was measured. The cell was also rotated about its central vertical axis so that a maximum value of v_h was achieved. It is seen from Fig. 1 that the measured GCB is a singly peaked function, whereas the BCG is approximately zero at all delay times (the BCG shows a slight hump at the noise level, and it is too small to be resolved). Figure 1 can be understood as follows. Because the seed particles first pass the green and then the blue beams, delaying $I_g(t)$ with a time interval equal to that for the particle to cross the two laser beams will give a nonzero intensity product, $\langle I_g(t')I_b(t'+t) \rangle$. For other delay times the average of the intensity product is zero, since the delay time does not match the beam crossing time. Obviously, for the same flow direction, BCG is zero because $I_b(t)$ is delayed in a wrong direction. The solid curve in Fig. 1 shows the fit to Eq. (2) with $v_0 = 0.89$ cm/s and $\sigma = 0.3$ cm/s. It is found that the measured $G_c(t)$ at different values of z and Ra can all be well fitted by Eq. (2). Figure 1 thus suggests that v_h is essentially unidirectional near the boundary, and its PDF $P(v)$ is of Gaussian form. Gaussian-like velocity PDF's have also been found in the central region of the cell [9]. The vertical velocity v_v is also measured near the boundary at various Ra . Within the sensitivity of the technique, we find v_v to be negligible. This confirms a previous observation [6] that near the boundary, v_h is the dominant component of the local velocity.

We now discuss $v_h(z)$ at various Ra . Figure 2(a) shows the measured $v_h(z)$ at $Ra = 9.24 \times 10^8$. The values of $v_h(z)$ were obtained by fitting the measured $G_c(t)$ by Eq. (2). It is seen that $v_h(z)$ increases with z for small values of z . After it reaches the maximum value v_m , $v_h(z)$ decays when z is further increased toward the cell center ($z = 9.8$ cm). Note that $v_h(z)$ in Fig. 2(a) does not decay to zero at the cell center. This is because $G_c(t)$ measures the particle velocity only in one direction, and like many other time-of-flight velocimeters, the dual-

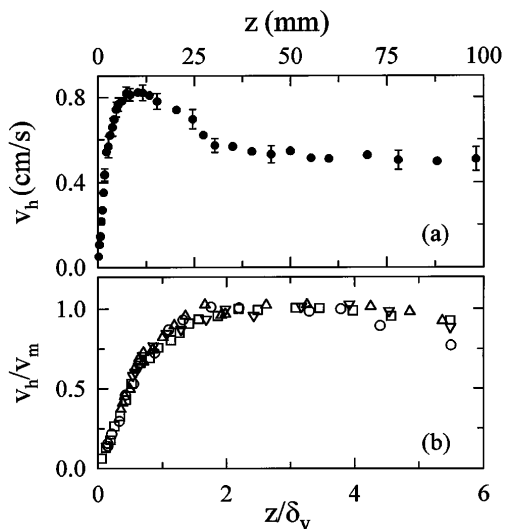


FIG. 2. (a) Measured horizontal velocity $v_h(z)$ as a function of the distance z from the bottom plate at $Ra = 9.24 \times 10^8$. (b) Scaled horizontal velocity profile $v_h(z)/v_m$ as a function of z/δ_v for four values of Ra : 2.86×10^8 (circles), 9.24×10^8 (squares), 3.6×10^9 (triangles), and 9.34×10^9 (inverted triangles).

beam method has a low-velocity cutoff v_c . Below v_c the seed particles will have an increasing probability to change their direction of motion (due to Brownian and turbulent diffusion) during their flight between the two laser beams. As a result, the particles may never cross the two parallel beams in succession and their motion will not be registered by $G_c(t)$. For our experimental setup, v_c is small ($<0.2v_h$) near the boundary, but it becomes significant at the cell center where the mean velocity $v_0 = 0$. Because of the velocity cutoff, the measured $G_c(t)$ at the cell center only samples large velocity fluctuations (rare events), and small velocity fluctuations (the most probable events) are left out. This explains why at the cell center it took a much longer time to accumulate $G_c(t)$ with good statistics. In fact, as we move the beams toward the cell center, the BCG gradually changes its functional form into a singly peaked function similar to the GCB shown in Fig. 1. In the central region the measured GCB and BCG become identical, indicating that the flow velocity fluctuates symmetrically in two opposite directions. From the above discussion, it becomes clear that the dual-beam method works best when v_0 is much larger than the standard deviation σ (e.g., $v_0 \geq 3\sigma$). The velocity boundary layer measurements reported in this Letter were all conducted under this ideal condition. It is found that when $v_0 \geq 3\sigma$, the fitted values of $v_h(z)$ from Eq. (2) are very close to those determined directly from the peak position of the measured $G_c(t)$.

As shown in Fig. 2(a), the measured $v_h(z)$ near the boundary can be well described by a linear function of z with a zero intercept (nonslip boundary condition). The slope of the linear function is the shear rate γ . The

thickness δ_v of the viscous boundary layer is defined as the distance at which the extrapolation of the linear part of $v_h(z)$ equals v_m , or simply $\delta_v = v_m/\gamma$. It is found that the measured velocity profiles $v_h(z)$ for different Ra can all be brought into coincidence, once the velocity $v_h(z)$ is scaled by v_m and the distance z is scaled by δ_v . The plot of $v_h(z)/v_m$ vs z/δ_v is found to remain invariant, and only v_m and δ_v change with Ra . Figure 2(b) shows typical $v_h(z)/v_m$ as a function of z/δ_v for four values of Ra . The scaling behavior of the measured $v_h(z)/v_m$ suggests that the law of the wall [10] applies to the velocity boundary layers in turbulent convection. However, there is a significant difference between thermal turbulence in a closed cell and turbulence in open flow systems such as in a pipe. As discussed in the above, the mean velocity in the core region of turbulent convection is zero, whereas in most open flow systems this velocity reaches maximum. The fact that the nonzero mean velocity is confined mainly in the near-wall region suggests that the size of the large-scale circulation (i.e., the cell height h) cannot be used as a second length scale much larger than δ_v for the asymptotic analysis [10] of the velocity boundary layers in turbulent convection. As a result, there is little range for the inertial sublayer, in which the velocity profile is of logarithmic form [10].

We now examine the Ra dependence of the characteristic quantities for the boundary layer: v_m , γ , and δ_v . The circles in Fig. 3 represent the measured v_m as a function of Ra . The data are well described by $v_m = (3.1 \pm 0.7) \times 10^{-5} Ra^{0.50 \pm 0.01}$ cm/s (upper solid line). If the Peclet number $Pe (=v_m h/\kappa)$ is chosen as a dimensionless velocity, we find from Fig. 3 that $Pe = 0.4Ra^{0.5}$. To understand the spatial structure of the flow field, we compare our velocity measurements with those near the sidewall of a cell far away from the upper and the lower plates [11]. The measured velocity near the sidewall is found to obey a power law of Ra , and the obtained exponent and amplitude are very close to our measured $v_m(Ra)$ near the boundary. With these two local measurements we conclude that the measured v_m is the speed of the large-scale circulation that sweeps over the surfaces of the cell and shears the thermal boundary layers [2]. Figure 2 clearly shows that this large-scale circulation is confined mainly in the near-wall region and has a width of $\sim 5\delta_v$, within which the velocity is approximately a constant. The direction of the circulation is found to remain unchanged during the measurements over the entire range of Ra . The power law behavior of the measured $v_m(Ra)$ could be explained if one assumes that v_m is proportional to the free-fall velocity $v_f \approx (\alpha g h \Delta T)^{1/2} \approx 1.9 \times 10^{-4} Ra^{1/2}$ cm/s. The fact that the measured v_m has a smaller amplitude than v_f can be attributed to the dissipations in the real system. In Fig. 3 we also plot the standard deviation $\sigma_m(Ra)$ for v_m (squares). The values of σ_m were obtained by fitting the measured $G_c(t)$ by Eq. (2). The lower solid line

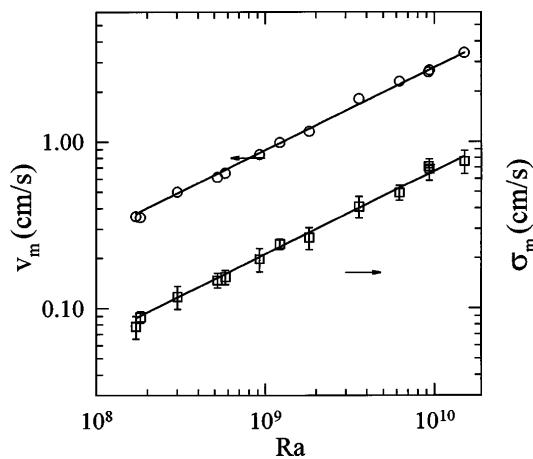


FIG. 3. Measured maximum horizontal velocity v_m (circles) and its standard deviation σ_m (squares) as a function of Ra. The solid lines are the power law fits.

represents the fit $\sigma_m = (7 \pm 4) \times 10^{-6} \text{Ra}^{0.50 \pm 0.04} \text{ cm/s}$. Figure 3 thus reveals that, for the large-scale circulation, the ratio of the standard deviation to the mean is $\sigma_m/v_m \approx 22\%$ and is independent of Ra. The measured power law exponent for $\sigma_m(\text{Ra})$ is close to that found at the cell center [9].

Figure 4(a) shows the measured shear rate γ as a function of Ra. The data are well described by $\gamma = (2.6 \pm 0.5) \times 10^{-6} \text{Ra}^{0.66 \pm 0.01} \text{ s}^{-1}$ (solid line). With the measured $\gamma(\text{Ra})$ and $\text{Nu}(\text{Ra})$, we find $\text{Nu} \sim \gamma^{0.44}$. This result does not support the scaling relation $\text{Nu} \sim \gamma^{1/3}$, which was suggested by a recent model [5]. In the model v_h was assumed to be independent of the horizontal coordinates, and a temperature boundary layer equation was obtained by further neglecting the temperature derivatives with respect to the horizontal coordinates. Recently, Ching [12] pointed out that the calculated temperature derivatives from the solution of the model are not small near the boundary, and therefore they cannot be ignored in the boundary layer equation. Figure 4(b) shows the measured δ_v as a function of Ra (circles). The upper solid line represents the fit $\delta_v = (10 \pm 2) \text{Ra}^{-(0.16 \pm 0.02)} \text{ cm}$. This result is consistent with the calculated $\delta_v(\text{Ra}) [= v_m(\text{Ra})/\gamma(\text{Ra})]$ directly from the measured v_m and γ . It is seen that δ_v decays smoothly as $\text{Ra}^{-0.16}$, and we did not observe any abrupt changes, as suggested by a recent temperature experiment [6]. In that experiment, a cutoff frequency from the temperature power spectrum was used to deduce the viscous boundary layer thickness indirectly. A recent direct numerical simulation of high-Ra convection also reported that no abrupt changes were observed in the scaling of the dissipation cutoffs [13]. In Fig. 4(b) we also plot the thermal boundary layer thickness δ_{th} (squares), which is obtained from the measured Nu using the well-tested relation $\delta_{th} = h/2\text{Nu}$ [6]. This thickness is well described by $\delta_{th} = 70.0 \text{Ra}^{-0.29} \text{ cm}$ (lower solid line). As shown in Fig. 4(b), the thermal boundary layer is nested within the

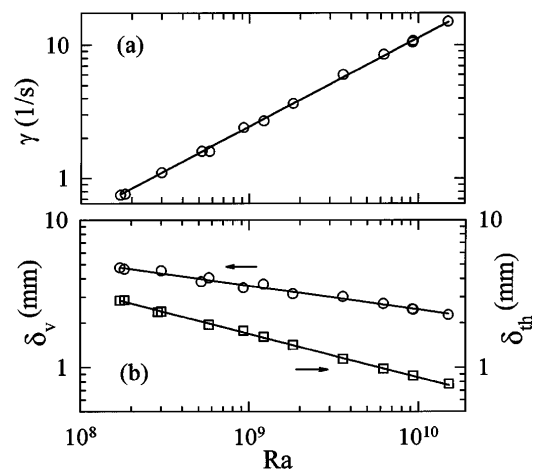


FIG. 4. (a) Measured shear rate γ versus Ra. The solid line shows the power law fit $\gamma = 2.6 \times 10^{-6} \text{Ra}^{0.66}$. (b) Measured viscous (circles) and thermal (squares) boundary layer thicknesses versus Ra. The solid lines represent the power law fits $\delta_v = 10 \text{Ra}^{-0.16} \text{ cm}$ and $\delta_{th} = 70.0 \text{Ra}^{-0.29} \text{ cm}$.

viscous boundary layer in our working range of Ra [5]. Clearly, if the current trend for $\delta_v(\text{Ra})$ and $\delta_{th}(\text{Ra})$ continues, the viscous and thermal boundary layers would not crossover at higher Ra.

We thank E. S. C. Ching and J. H. H. Perk for helpful discussions. Support of this work by the Research Grants Council (Hong Kong) is gratefully acknowledged. P. Tong was supported by the National Science Foundation under Grant No. DMR-9312398.

- [1] F. Heslot, B. Castaing, and A. Libchaber, *Phys. Rev. A* **36**, 5870 (1987); B. Castaing *et al.*, *J. Fluid Mech.* **204**, 1 (1989).
- [2] E. D. Siggia, *Annu. Rev. Fluid Mech.* **26**, 137 (1994).
- [3] T. H. Solomon and J. P. Gollub, *Phys. Rev. Lett.* **64**, 2382 (1990); *Phys. Rev. A* **43**, 6683 (1991).
- [4] F. Chilla, S. Ciliberto, and C. Innocenti, *Europhys. Lett.* **22**, 681 (1993).
- [5] B. I. Shraiman and E. D. Siggia, *Phys. Rev. A* **42**, 3650 (1990).
- [6] A. Tilgner, A. Belmonte, and A. Libchaber, *Phys. Rev. E* **47**, R2253 (1993); *Phys. Rev. Lett.* **70**, 4067 (1993); *Phys. Rev. E* **50**, 269 (1994).
- [7] K.-Q. Xia, Y.-B. Xin, and P. Tong, *J. Opt. Soc. Am. A* **12**, 1571 (1995).
- [8] H. Tanaka and H. Miyata, *Int. J. Heat Mass Transfer.* **23**, 1273 (1980).
- [9] Y. Shen, K.-Q. Xia, and P. Tong, *Phys. Rev. Lett.* **75**, 437 (1995).
- [10] H. Tennekes and J. L. Lumley, *A First Course in Turbulence* (MIT Press, Cambridge, 1972).
- [11] M. Sano, X.-Z. Wu, and A. Libchaber, *Phys. Rev. A* **40**, 6421 (1989); X.-Zu. Wu and A. Libchaber, *Phys. Rev. A* **45**, 842 (1992).
- [12] E. S. C. Ching (to be published).
- [13] R. M. Keer, A. Brandenburg, and J. R. Herring, *Bull. APS* **40**, 1928 (1995).